NANO LETTERS

Letter

Cite This: Nano Lett. 2019, 19, 6072−6077

pubs.acs.org/NanoLett

Nonlinear Metasurface Fresnel Zone Plates for Terahertz Generation and Manipulation

Eviatar Minerbi,*[,†,‡,§] Shay Keren-Zur,[†,‡] and Tal Ellenbogen[†,‡]

[†]Department of Physical Electronics, School of Electrical Engineering, [‡]Center for Light-Matter Interaction, and [§]Raymond and Beverly Sackler Faculty of Exact Sciences, School of Physics & Astronomy, Tel-Aviv University, Tel Aviv 6997801, Israel

ABSTRACT: We introduce a nanoengineered nonlinear metasurface based optical element that acts as an emitting Fresnel zone plate of terahertz (THz) waves. We show that the nonlinear zone plate generates broadband THz radiation and focuses each generated frequency on a different focal point along the optical axis. Therefore, a narrow beam waist and spectral selectivity of both the bandwidth and central frequency are achieved. Furthermore, we measure and analyze the temporal structure of the focused THz electric field and show that it comprises of few cycles with an axially varying carrier frequency in agreement with the calculated dispersion of the zone plate. This demonstration of controlled emission and focusing of THz waves opens the door for the development of a wide variety of additional holographic metasurface-based THz emitters and can lead to the development of efficient, active, integrated, and ultracompact optical devices for the THz spectral region.

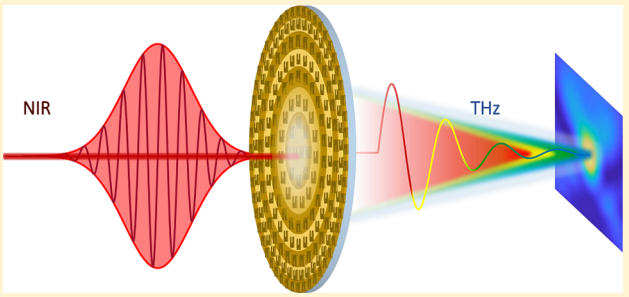

KEYWORDS: *Nonlinear metasurface (NLMS), Fresnel zone plate (FZP), terahertz (THz), manipulation*

Electromagnetic waves in the terahertz (THz) spectral regime, at frequencies ranging from about 0.1 to 10 THz, can be used for many important applications, including various types of nondestructive measurements,[1] imaging through optically opaque materials,[2] and for obtaining extended communication speeds.[3] However, there is still a lack of THz sources, detectors, and elements for manipulation that are functionally comparable to those in the optical or radio frequency regimes. This lack impedes the progress of research and the technology of THz waves.[4] However, it also drives the exploration of new means to overcome this important challenge. One promising direction that was studied recently is the use of artificially structured materials for the manipulation of THz radiation. Important functionalities that were obtained include polarization manipulation,[5] enhanced absorption,[6] mode multiplexing,[7] focusing,[8] and active-phase modulation.[9]

Furthermore, the possibility of generating THz radiation from nanostructured metal−dielectric surfaces, also called plasmonic metasurfaces, was recently introduced.[10−14] The metallic nanostructures that compose the plasmonic metasurfaces support resonances associated with collective free electron motion, called localized surface plasmon resonances (LSPRs). These resonances enhance and localize the electromagnetic (EM) field in the vicinity of the metallic nanostructures and also give rise to enhanced nonlinear interactions.[15] The generation of THz radiation from these structured surfaces was achieved either by ponderomotive acceleration of photoelectrons[10,11] or by optical rectification (OR) of ultrashort pulses.[12−14]

In principle, the THz-generating OR process, which is a second-order nonlinear process, is not supported by metals because of their centrosymmetric bulk structure. However, in plasmonic metasurfaces the symmetry break on the surface of the nanostructures, together with the high surface to volume ratio, and plasmonic field enhancements can lead to pronounced quadratic nonlinearities that can be used to generate light at new frequencies.[15−17] For example, split ring resonators (SRRs) on a subwavelength scale relative to the pump wavelength, which were proven to be useful for functional second-harmonic (SH) generation,[18−20] were also shown to support THz generation with an efficiency comparable to that of a 0.1-mm-thick ZnTe crystal.[13] It was shown that inverting their orientation introduces a π-phase shift to the locally generated light. This was used to demonstrate spatial control of the generated SH.[18,21] Very recently, it was shown that similar concepts also allow us to obtain unprecedented control capabilities over the spatiotemporal structure of broadband THz radiation emitted from nonlinear metasurfaces (NLMS).[14] These capabilities were shown for binary phase manipulation with a fixed amplitude, whereas both phase and amplitude control were very recently studied only theoretically.[22] Here we demonstrate experimentally the ability to simultaneously vary the amplitude of the generated pulse and achieve phase control, enabling enhanced manipulation of the spatiotemporal structure of the emitted

Received: May 14, 2019
Revised: July 25, 2019
Published: July 29, 2019

DOI: 10.1021/acs.nanolett.9b01970
Nano Lett. 2019, 19, 6072−6077

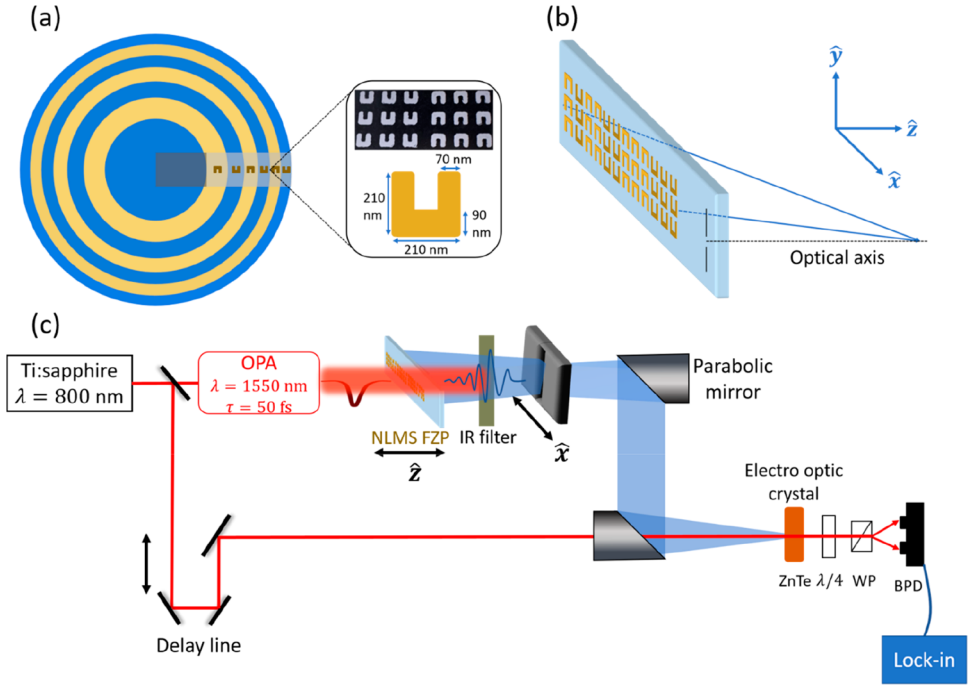

Figure 1. (a) Illustration of a 2D FZP. The highlighted area marks the fabricated sample constructed from zones 2−7 (one side, 1D). Magnified frame shows a SEM image of two neighboring regions in the FZP and the SRR dimensions. (b) Illustration of the wave propagation to the focal plane from the fabricated sample. The vertical marks indicate the optical axis of the FZP. (c) Experimental setup. Ti:Sapp, amplified titanium sapphire laser. OPA, optical parametric amplifier. ZnTe, 0.5 mm (110-cut) crystal. WP, Wollaston prism. BPD, balanced photodiode.

THz pulse. Such shaped single- or few-cycle THz pulses may permit new functionalities in time-of-flight noninvasive imaging for various applications, including biomedicine,[23] security,[24] and art.[25,26] The ability to generate and manipulate the THz radiation on a single surface has many advantages as it circumvents some fundamental issues that are encountered by conventional THz generation and manipulation schemes that need to be compensated for, such as materials dispersion,[27] phase matching,[28,29] and phonon absorption.[30] Indeed, a variety of methods to overcome these issues exist; however, they usually require a careful design and are not applicable to all materials.[28,31] Therefore, developing new ways to generate and control THz radiation may open the door to construct new and improved optical elements for the THz regime.

One of the first, most important, and most widely used classes of optical elements are lenses, which exist in almost every optical system. Specifically, most of the aforementioned THz applications require focusing the THz radiation to specific locations of interest. To meet this need, here we develop a nanostructured nonlinear THz Fresnel zone plate (FZP) lens for broadband THz generation and spectrally dispersive focusing. We study numerically and experimentally the performance of the element and show that it generates multicycle THz pulses and focuses desired frequencies into different focal lengths, hence providing a new promising means to generate and manipulate THz radiation by a single, ultrathin, and easily integrated element.

Figure 1a shows the design of the NLMS-based FZP. The NLMS-FZP is constructed from 40-nm-thick gold SRRs and is made of zones with alternating orientation of the SRRs. The radius of the nth zone is given by

$$R_n = \sqrt{n\lambda_{\mathrm{THz}} f + \frac{n^2 \lambda_{\mathrm{THz}}^2}{4}} \quad (1)$$

where λ_{THz} is the THz wavelength and f is the distance to the focal point. Using eq 1 to calculate the FZP size required to focus a wave with a central frequency of 1 THz (λ = 0.3 mm) to a focal point located at f = 30 mm shows that $R_7 \approx 8$ mm. On the other hand, the features of the SRRs that compose the nonlinear metasurface are on the order of ∼70 nm (inset in Figure 1a). Therefore, the conventional electron-beam lithography nanofabrication process of a complete centimeter-scale FZP with such nanometric resolution is extremely long and difficult, and misalignments can be easily made. To overcome this problem, while studying the characteristics of such a FZP, we decided to fabricate and test a smaller one-sided off-axis FZP with seven zones of alternating SRRs (n = 2:7; see Figure 1a and Methods). A ray optics representation of the focusing from such a FZP is shown in Figure 1b. The sample is illuminated by a near-infrared (NIR) ultrashort pulse, with a central wavelength of 1550 nm, a pulse duration of ∼50 fs, an average power of ∼60 mW, and a beam diameter of ∼6.8 (1.7) mm in the x (y) direction (Methods). The THz signal is detected by an electro-optic sampling technique (Figure 1c and Methods).[32,33] To enhance the nonlinear interaction, the SRRs were designed to support LSPR at the wavelength of the pump, ∼1550 nm.[34] Each uniform zone generates a broadband single-cycle THz pulse.[13,14] The alternating phase of the THz pulses generated in the different zones of the sample due to the inversion of the SRRs creates an interference pattern. Consequently, different frequencies focus at different distances along the optical axis (i.e., z axis) according to eq 1.

To measure the focusing properties of the nonlinear THz FZP, we use a filtering slit as shown in Figure 1c. The placement of the slit on the optical axis allows us to collect mainly the focused frequency. The slit was placed at the focal point of the first parabolic mirror (NA = 0.25) in order to achieve the most efficient collection of light. In addition, the

DOI: 10.1021/acs.nanolett.9b01970
Nano Lett. 2019, 19, 6072−6077

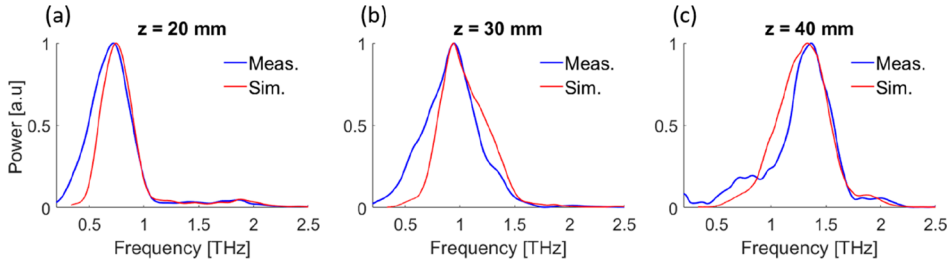

Figure 2. Simulated (red lines) and measured (blue lines) on-axis THz spectra for different focal distances: (a) z = 20 mm, (b) z = 30 mm, and (c) z = 40 mm.

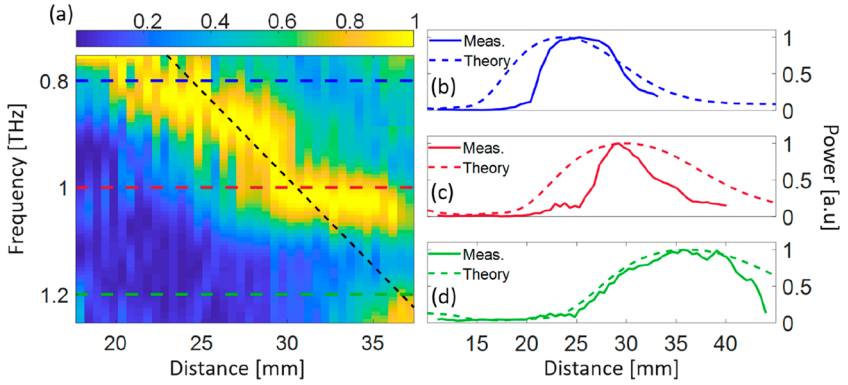

Figure 3. (a) Normalized THz power for different frequencies as a function of the distance from the FZP. The dashed line is the theoretical trajectory of frequency vs distance. (b–d) Power as a function of distance for (b) 0.8 THz, theoretical f = 25 mm; (c) 1 THz, theoretical f = 30 mm; and (d) 1.2 THz, theoretical f = 35 mm.

NLMS-FZP was mounted on a linear translation stage that can be moved along the z axis. Tuning the distance between the FZP and the slit allows us to measure the frequency dispersion along the optical axis. The generated THz field was measured with a time domain spectroscopy measurement (Figure 1 and Methods). Therefore, the intensity of the pulse together with its temporal structure was detected. The spectrum of the THz signal was retrieved by Fourier transform. To measure the spatial profile of the generated pulse, the slit was also slightly moved along the x axis (Figure 1c). Because the movement along the x axis was much smaller than the distance to the parabolic mirror (~1 mm vs ~10 cm), the collection efficiency reduction for translations along the x axis (and out of the focal point of the parabolic mirror) was neglected.

Figure 2 shows the measured and simulated (Methods) on-axis THz spectrum for different distances from the FZP (z = 20 mm, 30 mm, 40 mm). To simulate accurately the wave propagation of the THz radiation after the FZP, we need to take into account the THz emission spectrum from a uniform NLMS. This was done by adding a weight function based on a measured spectrum (Methods) for the different frequencies generated by the NLMS. It can be seen that there is very good agreement between the experimental measurements and the numerical simulations. The measured and simulated results show that the lower frequencies are focused at short distances while the high frequencies are focused further away, as implied by eq 1.

To show the full effect of spectral lensing of the generated THz radiation, we plot in Figure 3a the detected power vs frequency and distance after the FZP. The dashed black line shows the theoretical frequency-focus relation which is calculated from eq 1, under the approximation of $\lambda \ll f$, to be $\nu_{\mathrm{THz}} = \frac{7c}{R_7^2} \times f$, where ν_{THz} is the frequency, c is the speed of light, and f is the distance to the focal point. It can be seen that there is good agreement between the theoretical prediction of the focusing properties of the nonlinear THz FZP and the measured results. The subtle steplike behavior of the measured power vs frequency and distance is due to the fact that the generation of the THz radiation is not uniform along all frequencies and because of the partial FZP nature of our fabricated sample. In addition, there might have been slight misalignments in the experiment. A complete 1D or 2D NLMS-FZP will result in smoother results. Moreover, increasing the number of zones will lead to better spectral resolution because it is governed by the smallest zone of the FZP. In Figure 3b–d, we present the measured and simulated power vs distance for 0.8, 1, and 1.2 THz, respectively. It can be seen that the simulations and measurements are in relatively good agreement in terms of location and depth of focus.

Next we characterized the spatial profile of the focused THz beam. This measurement was performed by moving the slit along the x axis and measuring the collected THz. The THz power profile measured at z = 30 mm for 0.9 THz is shown in Figure 4a. It can be seen that the THz energy is focused to a Gaussian-like profile with a full width at half-maximum (fwhm) of ~0.72 mm. This fits the expected fwhm generated by the FZP which can be calculated by $w_{\mathrm{fwhm}} \approx 1.22 \times \Delta r = 0.735$ mm, where $\Delta r = r_7 - r_6$.

Since we scan along the x axis at the focal point of a specific frequency, one may intuitively expect a focusing effect for the corresponding frequency, while the other frequencies are not focused. To obtain a comprehensive picture of the focusing behavior of the nonlinear FZP, Figure 4b shows the full spectral power profile. It can be seen that a frequency-dependent lateral shift is measured rather than a focusing effect for a specific frequency alone. This shift occurs as a result of

DOI: 10.1021/acs.nanolett.9b01970
Nano Lett. 2019, 19, 6072–6077

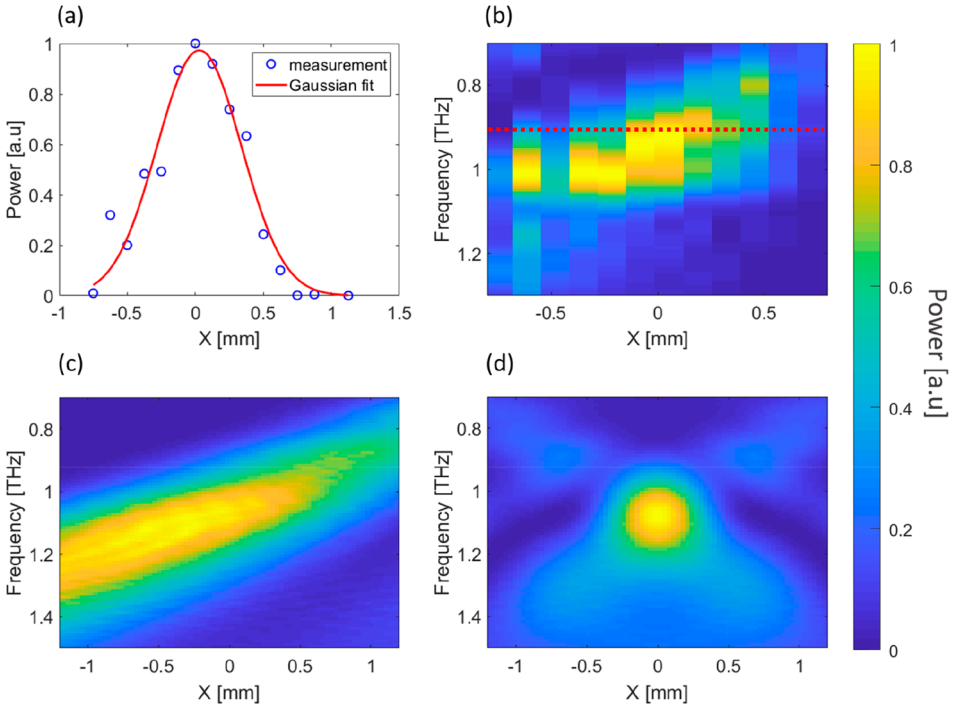

Figure 4. Focused beam profile. (a) Measured beam profile at 0.9 THz (blue dots) and a Gaussian fit (red line). (b) Measured beam profile at different frequencies. The red dashed line represents the frequency plotted in a. (c and d) Simulations of the frequency-dependent beam profile for one-sided and two-sided 1D FZP, respectively. Note that all figures share the same normalized color scale.

the fact that we fabricated a one-dimensional, one sided off-axis FZP. Simulations of the performance of such an FZP agree well with the measurement, as shown in Figure 4c. Simulations of one-dimensional, two-sided FZP with seven zones presented in Figure 4d clearly show that a symmetric focusing effect is obtained in this case.

When considering a diffractive optical element, it is often convenient to analyze the frequency response of the interacting waves. However, examining the temporal behavior may improve our understanding of the complete physical picture and allow us to envision potential applications, especially in the case of ultrashort pulses. Therefore, in the following section we discuss the temporal structure of the generated THz. The measured temporal structure of the on-axis THz field for different distances from the FZP is presented in Figure 5a. It can be seen that the on-axis THz field consists of a few-cycle pulse that changes its carrier frequency along the optical axis. The few-cycle structure agrees well with the calculated relative time of arrival of waves originating in different consecutive zones on the FZP (represented by dashed lines). To obtain more insight, in Figure 5b–e we compare between the structure of the generated THz pulse from a uniform SRR array and from a FZP at a distance of $z = 30$ mm. The signal in time domain is presented in Figure 5b,d, and the respective amplitude spectra are presented in Figure 5c,e. It can be seen that the single cycle pulse generated by the uniform SRR array becomes a few cycle pulse in the case of the FZP. This effect is due to the direct space to time mapping between the NLMS structure and the generated pulse as theoretically predicted by Keren-Zur et al.[22] The different regions of the NLMS generate single-cycle pulses that constructively interfere with a time delay related to their origin on the metasurface (i.e., the distance from their origin to the measurement slit divided by the speed of light). A similar effect was shown with a NLMS photonic crystal in which the periodic structure of the NLMS was mapped into a periodic pulse shape.[14] However, unlike a one-dimensional photonic crystal, the zones in a FZP are not the same size, thus leading to weaker cycle generation from the outer zones. Therefore, we obtain phase control for the generated THz pulse while its amplitude varies. This feature opens the door for more sophisticated ultrathin devices, enabling full control of both phase and amplitude.

In conclusion, we have experimentally demonstrated and studied a nonlinear metasurface-based lens that is able to generate broadband THz radiation and simultaneously selectively focus its different frequency components along the optical axis. These results are obtained with excellent agreement between the theoretical predictions and our measurements. We show that, very interestingly, the on-axis-focused radiation takes the form of few-cycle pulses with changing carrier frequencies. Fabricating a full THz emitting lens instead of a one-sided 1D lens that was used here for proof of concept will further improve the performance, and theoretically, there is no limitation on reaching the diffraction limit. Moreover, additional THz manipulation is possible by the careful design of the FZP. For example, efficiency enhancement,[35] fixed foci at different wavelengths[36,37] and modulation of the spatial phase[38] can be achieved. Considering the plethora of important applications of THz waves along with the challenges of generating and controlling THz radiation, we believe that these NLMS-based THz lenses may be attractive for various spectroscopic and imaging applications. Moreover, because the demonstrated FZP belongs to the large family of holographic optical elements, this demonstration motivates the development of additional holographic metasurface-based THz emitters that can be efficient, active, and integrated in ultracompact optical devices for pushing forward THz science and technology.

DOI: 10.1021/acs.nanolett.9b01970
Nano Lett. 2019, 19, 6072–6077

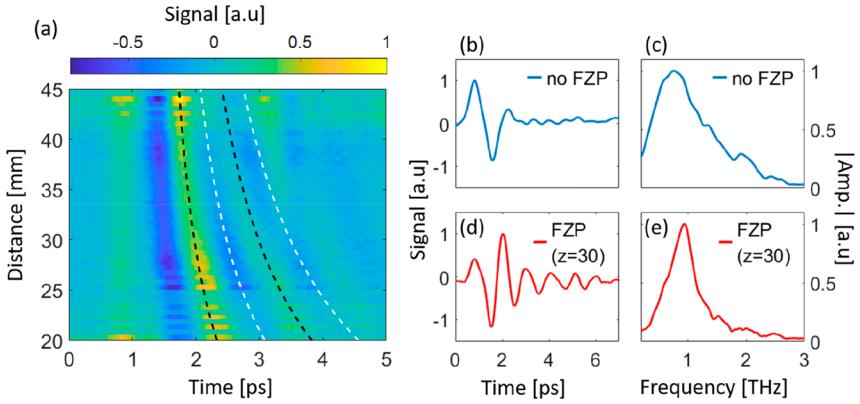

Figure 5. Temporal structure of the generated on-axis THz pulses. (a) Measured temporal structure of the THz field vs distance from the FZP. Dashed lines represent the calculated relative time of arrival of waves emitted from consecutive zones with alternating SRR orientation as black and white lines. (b–e) Comparison of the measured temporal structure (a and d) and amplitude spectrum (c and e) of the generated THz pulse from a uniform NLMS and an FZP NLMS, respectively, for a distance of z = 30 mm.

METHODS

Experimental Setup. An ultrashort pulse (35 fs, 800 nm central wavelength, 2 kHz repetition rate, 3.5 mJ pulse energy) emerging from a Ti:sapphire amplifier (Spectra Physics Solstice ACE) passes through a beam splitter. The main portion of the beam is used to pump an optical parametric amplifier (OPA- Spectra Physics TOPAS) to generate NIR radiation at a central wavelength of 1550 nm with a pulse duration of about 50 fs. The NIR beam is then widened in the x direction (X4 magnification) and illuminates the NLMS with an average power of 60 mW (after chopper) and a beam diameter of ∼6.8 mm in the x direction (∼1.7 mm in the y direction). The residual transmitted NIR radiation is filtered out by a Teflon window. The THz signal is spatially filtered by a slit located at the focal point of a parabolic mirror (NA = 0.25). The NLMS is mounted on a stage moving along the optical axis. A small portion of the amplifier pulse is used as a probe for the THz signal by electro-optic sampling with a 0.5-mm-thick ZnTe crystal. The THz field induces birefringence in the crystal, which consequently rotates the probe polarization. A delay line is used on the optical axis of the probe in order to temporally scan the THz pulse. The ZnTe crystal is followed by a quarter wave plate, a Wollaston prism, and a balanced photodiode in order to detect polarization modifications of the probe. The balanced photodiode signal due to the THz field is then detected by a lock-in amplifier (Stanford Research Systems SR830) coupled to a mechanical chopper located on the pump beam, which reduces the repetition rate on the NLMS to 1 kHz. The delay line, scanning stages, chopper, and lock-in amplifier were automatically controlled using Labview.

Sample Fabrication. The indium tin oxide-coated glass substrate was cleaned by sonication in acetone and isopropyl alcohol (IPA) and dried using a dry stream of N_2. The clean substrate was spin-coated with polymethyl methacrylate (PMMA A4) and then baked at 180 °C on a hot plate for 1 min. The FZP constructed from the SRRs was written by an electron-beam lithography system (Raith 150-II) at 20 kV. The patterned substrate was developed by immersion in cooled (4 °C) MIBK/IPA 1:3 for 1 min, followed by drying under a dry stream of N_2. A layer of 3 nm Ti was evaporated, followed by 37 nm of Au. The remaining resist was lifted off in acetone and dried under a dry stream of N_2. The SRRs had typical base and arm lengths of ∼210 nm and a width of 70 nm.

THz Propagation Simulations. The simulations were implemented using MATLAB. The broadband pulse was defined by adding a weight function from a measured spectrum of the THz field (Figure 5c). The electric field over the excited NLMS plane was defined for each frequency to be its spectral amplitude with a sign matching the orientation of the SRR on the NLMS and zero outside the NLMS. The slit was simulated by adding a rectangular transfer function with a width matching the width of the slit. The spatial Fourier transform of the field was propagated along the z axis separately for each frequency. By inverse Fourier transform of the frequency axis, the spatiotemporal field was reconstructed.

AUTHOR INFORMATION

Corresponding Author

*E-mail: minerbi@mail.tau.ac.il.

ORCID

Eviatar Minerbi: 0000-0002-1874-4919

Notes

The authors declare no competing financial interest.

ACKNOWLEDGMENTS

This publication is part of a project that has received funding from the European Research Council (ERC) under the European Union's Horizon 2020 research and innovation program (grant agreement no. 715362). S.K.Z. acknowledges support from the Tel Aviv University Center for Renewable Energy President Scholarship for Outstanding Ph.D. Students and support from the Israel Ministry of Science & Technology Scholarship for Ph.D. students in the applied sciences.

REFERENCES

(1) Zhong, S. Progress in Terahertz Nondestructive Testing: A Review. *Front. Mech. Eng.* **2019**, *14* (3), 273–281.

(2) Mittleman, D. M. Twenty Years of Terahertz Imaging [Invited]. *Opt. Express* **2018**, *26* (8), 9417–9431.

(3) Koenig, S.; Lopez-Diaz, D.; Antes, J.; Boes, F.; Henneberger, R.; Leuther, A.; Tessmann, A.; Schmogrow, R.; Hillerkuss, D.; Palmer, R.; et al. Wireless Sub-THz Communication System with High Data Rate. *Nat. Photonics* **2013**, *7*, 977.

(4) Mittleman, D. M. Perspective: Terahertz Science and Technology. *J. Appl. Phys.* **2017**, *122* (23), 230901.

DOI: 10.1021/acs.nanolett.9b01970
Nano Lett. 2019, 19, 6072–6077

(5) Cong, L.; Srivastava, Y. K.; Zhang, H.; Zhang, X.; Han, J.; Singh, R. All-Optical Active THz Metasurfaces for Ultrafast Polarization Switching and Dynamic Beam Splitting. *Light: Sci. Appl.* **2018**, *7*, 28.
(6) Tao, H.; Bingham, C. M.; Strikwerda, A. C.; Pilon, D.; Shrekenhamer, D.; Landy, N. I.; Fan, K.; Zhang, X.; Padilla, W. J.; Averitt, R. D. Highly Flexible Wide Angle of Incidence Terahertz Metamaterial Absorber: Design, Fabrication, and Characterization. *Phys. Rev. B: Condens. Matter Mater. Phys.* **2008**, *78* (24), 241103.
(7) Karl, N. J.; McKinney, R. W.; Monnai, Y.; Mendis, R.; Mittleman, D. M. Frequency-Division Multiplexing in the Terahertz Range Using a Leaky-Wave Antenna. *Nat. Photonics* **2015**, *9*, 717.
(8) Yi, H.; Qu, S.-W.; Chen, B.-J.; Bai, X.; Ng, K. B.; Chan, C. H. Flat Terahertz Reflective Focusing Metasurface with Scanning Ability. *Sci. Rep.* **2017**, *7* (1), 3478.
(9) Liu, L.; Zhang, X.; Kenney, M.; Su, X.; Xu, N.; Ouyang, C.; Shi, Y.; Han, J.; Zhang, W.; Zhang, S. Broadband Metasurfaces with Simultaneous Control of Phase and Amplitude. *Adv. Mater.* **2014**, *26* (29), 5031−5036.
(10) Welsh, G. H.; Wynne, K. Generation of Ultrafast Terahertz Radiation Pulses on Metallic Nanostructured Surfaces. *Opt. Express* **2009**, *17* (4), 2470−2480.
(11) Polyushkin, D. K.; Hendry, E.; Stone, E. K.; Barnes, W. L. THz Generation from Plasmonic Nanoparticle Arrays. *Nano Lett.* **2011**, *11* (11), 4718−4724.
(12) Tymchenko, M.; Sebastian Gomez-Diaz, J.; Lee, J.; Belkin, M.; Alu, A. Highly-Efficient THz Generation Using Nonlinear Plasmonic Metasurfaces. *J. Opt.* **2017**, *19*, 104001.
(13) Luo, L.; Chatzakis, I.; Wang, J.; Niesler, F. B. P.; Wegener, M.; Koschny, T.; Soukoulis, C. M. Broadband Terahertz Generation from Metamaterials. *Nat. Commun.* **2014**, *5*, 3055.
(14) Keren-Zur, S.; Tal, M.; Fleischer, S.; Mittleman, D. M.; Ellenbogen, T. Generation of Spatiotemporally Tailored Terahertz Wavepackets by Nonlinear Metasurfaces. *Nat. Commun.* **2019**, *10* (1), 1778.
(15) Kauranen, M.; Zayats, A. V. Nonlinear Plasmonics. *Nat. Photonics* **2012**, *6*, 737.
(16) Ciracì, C.; Poutrina, E.; Scalora, M.; Smith, D. R. Origin of Second-Harmonic Generation Enhancement in Optical Split-Ring Resonators. *Phys. Rev. B: Condens. Matter Mater. Phys.* **2012**, *85* (20), 201403.
(17) Klein, M. W.; Enkrich, C.; Wegener, M.; Linden, S. Second-Harmonic Generation from Magnetic Metamaterials. *Science (Washington, DC, U. S.)* **2006**, *313* (5786), 502−504.
(18) Segal, N.; Keren-Zur, S.; Hendler, N.; Ellenbogen, T. Controlling Light with Metamaterial-Based Nonlinear Photonic Crystals. *Nat. Photonics* **2015**, *9*, 180.
(19) Krasnok, A.; Tymchenko, M.; Alù, A. Nonlinear Metasurfaces: A Paradigm Shift in Nonlinear Optics. *Mater. Today* **2018**, *21*, 8.
(20) Li, G.; Zhang, S.; Zentgraf, T. Nonlinear Photonic Metasurfaces. *Nat. Rev. Mater.* **2017**, *2*, 17010.
(21) Keren-Zur, S.; Avayu, O.; Michaeli, L.; Ellenbogen, T. Nonlinear Beam Shaping with Plasmonic Metasurfaces. *ACS Photonics* **2016**, *3* (1), 117−123.
(22) Keren-Zur, S.; Ellenbogen, T. Direct Space to Time Terahertz Pulse Shaping with Nonlinear Metasurfaces. *Opt. Express* **2019**, *27* (15), 20837−20847.
(23) Guillet, J. P.; Recur, B.; Frederique, L.; Bousquet, B.; Canioni, L.; Manek-Hönninger, I.; Desbarats, P.; Mounaix, P. Review of Terahertz Tomography Techniques. *J. Infrared, Millimeter, Terahertz Waves* **2014**, *35* (4), 382−411.
(24) Federici, J. F.; Schulkin, B.; Huang, F.; Gary, D.; Barat, R.; Oliveira, F.; Zimdars, D. THz Imaging and Sensing for Security Applications—Explosives, Weapons and Drugs. *Semicond. Sci. Technol.* **2005**, *20* (7), S266−S280.
(25) Gomez-Sepulveda, A. M.; Hernandez-Serrano, A. I.; Radpour, R.; Koch-Dandolo, C. L.; Rojas-Landeros, S. C.; Ascencio-Rojas, L. F.; Zarate, A.; Hernandez, G.; Gonzalez-Tirado, R. C.; Insaurralde-Caballero, M.; et al. History of Mexican Easel Paintings from an Altarpiece Revealed by Non-Invasive Terahertz Time-Domain Imaging. *J. Infrared, Millimeter, Terahertz Waves* **2017**, *38* (4), 403−412.
(26) Koch-Dandolo, C. L.; Filtenborg, T.; Fukunaga, K.; Skou-Hansen, J.; Jepsen, P. U. Reflection Terahertz Time-Domain Imaging for Analysis of an 18th Century Neoclassical Easel Painting. *Appl. Opt.* **2015**, *54* (16), 5123−5129.
(27) Wang, F.; Nong, H.; Fobbe, T.; Pistore, V.; Houver, S.; Markmann, S.; Jukam, N.; Amanti, M.; Sirtori, C.; Moumdji, S.; et al. Short Terahertz Pulse Generation from a Dispersion Compensated Modelocked Semiconductor Laser. *Laser Photon. Rev.* **2017**, *11* (4), 1700013.
(28) Lu, J.; Lee, S.-H.; Li, X.; Lee, S.-C.; Han, J.-H.; Kown, O.-P.; Nelson, K. A. Efficient Terahertz Generation in Highly Nonlinear Organic Crystal HMB-TMS. *Opt. Express* **2018**, *26* (23), 30786−30794.
(29) Avetisyan, Y.; Tonouchi, M. Terahertz Generation in Quasi-Phase-Matching Structure Formed by a Phase Mask. *Opt. Lett.* **2012**, *37* (19), 4155−4157.
(30) Ferguson, B.; Zhang, X.-C. Materials for Terahertz Science and Technology. *Nat. Mater.* **2002**, *1* (1), 26−33.
(31) Hebling, J.; Almási, G.; Kozma, I. Z.; Kuhl, J. Velocity Matching by Pulse Front Tilting for Large-Area THz-Pulse Generation. *Opt. Express* **2002**, *10* (21), 1161−1166.
(32) Wu, Q.; Zhang, X.-C. Free-space Electro-optic Sampling of Terahertz Beams. *Appl. Phys. Lett.* **1995**, *67* (24), 3523−3525.
(33) Lee, Y.-S. *Principles of Terahertz Science and Technology* 2009. DOI: 10.1007/978-0-387-09540-0.
(34) Novotny, L. Effective Wavelength Scaling for Optical Antennas. *Phys. Rev. Lett.* **2007**, *98* (26), 266802.
(35) Jouade, A.; Himdi, M.; Lafond, O. Fresnel Lens at Millimeter-Wave: Enhancement of Efficiency and Radiation Frequency Bandwidth. *IEEE Trans. Antennas Propag.* **2017**, *65* (11), 5776−5786.
(36) Doskolovich, L. L.; Bezus, E. A.; Morozov, A. A.; Osipov, V.; Wolffsohn, J. S.; Chichkov, B. Multifocal Diffractive Lens Generating Several Fixed Foci at Different Design Wavelengths. *Opt. Express* **2018**, *26* (4), 4698−4709.
(37) Eisenbach, O.; Avayu, O.; Ditcovski, R.; Ellenbogen, T. Metasurfaces Based Dual Wavelength Diffractive Lenses. *Opt. Express* **2015**, *23* (4), 3928−3936.
(38) Lin, L.; Goh, X. M.; McGuinness, L. P.; Roberts, A. Plasmonic Lenses Formed by Two-Dimensional Nanometric Cross-Shaped Aperture Arrays for Fresnel-Region Focusing. *Nano Lett.* **2010**, *10* (5), 1936−1940.

DOI: 10.1021/acs.nanolett.9b01970
Nano Lett. 2019, 19, 6072−6077